Journal of Materials Chemistry A

Accepted Manuscript

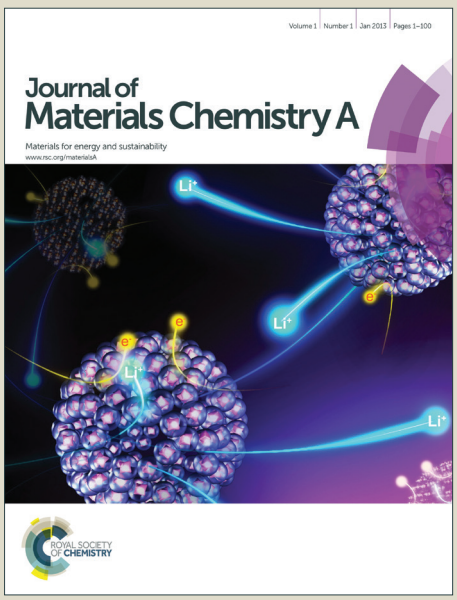

ROYAL SOCIETY OF CHEMISTRY

www.rsc.org/materialsA

Journal of Materials Chemistry A

Dynamic Article Links ►

Cite this: DOI: 10.1039/c0xx00000x

www.rsc.org/xxxxxx

ARTICLE TYPE

AgBr Quantum Dots Decorated Mesoporous Bi_2WO_6 Architectures with Enhanced Photocatalytic Activities for Methylene Blue

Danjun Wang,[a, b] Li Guo,[b] Yanzhong Zhen,[a, b] Linlin Yue,[b] Ganglin Xue,[a]* and Feng Fu[b]*

Received (in XXX, XXX) Xth XXXXXXXXX 20XX, Accepted Xth XXXXXXXXX 20XX
DOI: 10.1039/b000000x

The spherical mesoporous nest-like Bi_2WO_6 nanoarchitectures with scales of 2~4 μm were prepared via a hydrothermal process, and AgBr quantum dots (QDs) were decorated on the surface of Bi_2WO_6 to form a novel p-n AgBr/ Bi_2WO_6 heterojunction via a followed facile precipitation-deposition process. Evidence of AgBr QDs decorated mesoporous nest-like Bi_2WO_6 nanoarchitectures was obtained from XRD, XPS, FE-SEM and HR-TEM, which reveal monodispersed AgBr QDs with the average size of about 10 nm were deposited on the surface of the three-demsional Bi_2WO_6 nanoarchitectures. The photocatalytic activities of the samples were evaluated by the photodegradation of methylene blue dye (MB) and phenol under visible light irradiation. The results showed that AgBr QDs decoration great improved the photocatalytic activity of Bi_2WO_6, and the content of deposited AgBr nanodots has an impact on the catalytic activity of Bi_2WO_6. The 2.0at%AgBr-loaded Bi_2WO_6 sample exhibited the best photocatalytic activity for decolorization of MB. It is elucidated that AgBr/Bi_2WO_6 is able to generate superoxide radical anions in aqueous aerated solution, but no hydroxyl radicals are formed. In addition, the mechanism for the enhancement photocatalytic activity of AgBr/Bi_2WO_6 was also investigated by comparison of their PL spectra. The catalytic efficiency enhancement of the p-n AgBr/Bi_2WO_6 heterojunctions relative to pure Bi_2WO_6 can be attributed to the formation of heterojunctions between AgBr QDs and Bi_2WO_6, which suppress the recombination of photogenerated electron-hole pairs. The test of radical scavengers confirmed that $O_2^{\bullet -}$ was the main reactive species during the photocatalytic process.

[1] 1 Introduction

During the past decades, photocatalysis for environmental pollutants photodecomposition and hydrogen generation for water under solar light irradiation has attracted increasing interest.[1-3] Titanium dioxide (TiO_2) has been extensively studied for its largely available, inexpensive, non-toxic and relatively high chemical stability. However, TiO_2-based photocatalytic technology has not yet been used in application to industrial wastewater treatment due to its relatively inefficient quantum yield and the wide band gap.[4-5] Up to now, the most studied strategy to develop more efficient visible photocatalyst is to extend the absorption of TiO_2 in the visible range through different modification methods like TiO_2 doped with nonmetal element.[6-9] Unfortunately, the method used for doping element is not fully controlled, and low thermal stability of these compounds limits their applications. Moreover, these dopants may act as recombination centers between photogenerated electrons and holes and consequently decrease photocatalytic efficiency.[10-11] The expected improvement are somewhat limited, and therefore, the alternative strategy is to develop more efficient photocatalysis materials with visible light responsive, which is urgent and indispensable.[12-13]

As known to all, photocatalytic process involves the energy generation of charge carriers, such as electrons and holes induced by light, an ideal photocatalyst should have both a wide photoabsorption range and a low recombination rate of the photogenerated charge carriers. Therefore, it is necessary to develop effective way to improve the charge separation efficiency and extend the solar radiation spectral responsive range. Recently, some novel semiconductor heterojunction has been designed and fabricated by coupling a narrow band gap semiconductor over another photocatalyst. [14-16] Semiconductors heterojunction could decrease the recombination rate of photogenerated electron and holes and thus have been widely

[a]*Key Laboratory of Synthetic and Natural Functional Molecule Chemistry, Department of Chemistry (Ministry of Education), Northwest University, Xi'an, 710069, China. xglin@163.com +86-29-88302604*
[b]*College of Chemistry &Chemical Engineering, Yan'an University, Shaanxi Key Laboratory of Chemical Reaction Engineering, Yan'an 716000, China. E-mail: FengFu@126.com +86-911-2332224*
†Electronic Supplementary Information (ESI) available: See DOI: 10.1039/b000000x/

used to improve the photocatalytic activity of photocatalyst, which nas turned out to be an effective approach.[17-24]

Being one of the most important photocatalyst, bismuth tungstate (Bi_2WO_6) has received particular attention recently owing to its excellent photocatalytic property.[25-29] Unfortunately, there are two mainly drawbacks which limit the application of Bi_2WO_6 photocatalyst. Firstly, bare-Bi_2WO_6 exhibits photoabsorption properties from UV to visible light with wavelength of shorter than about 450 nm. Secondly, the rapid recombination of photoinduced electron and holes pairs seriously limits the light energy-conversion efficiency. Therefore, the way to broaden the range of visible-light photoresponsive and enhance the separation of photogenerated carriers of Bi_2WO_6 is important in maximizing the photocatalytic efficiency. In recent years, many strategies have been adopted to improve this situation. One strategies is to design and synthesize 3D nanostructured Bi_2WO_6 with large specific surface area.[30-41] Other efforts have been made on metal and non-metal elements doping.[42-45] Besides morphology controlling and doping Bi_2WO_6 with elements for improving the photocatalytic activity, fabrication of heterostructured Bi_2WO_6 with different carriers or different band gap has turned to be another effective approach.[46-51]

Recently, our group has successfully synthesized 3D nest-like mesoporous Bi_2WO_6 architectures by a hydrothermal method without any additives,[52] and Ag nanoparticles were deposited on the surface of Bi_2WO_6 *via* a following facile photoreduction process. The photocatalysis experimental results revealed that Ag-loaded Bi_2WO_6 exhibited high photocatalytic activity in both the decolorization of RhB and desulfurization of thiophene compared with pure Bi_2WO_6 and $TiO_{2-x}N_x$.[53] Wong et al. have reported a semiconductor-based AgBr-Ag-Bi_2WO_6 nanojunction system, where both AgBr and Bi_2WO_6 are used as visible-light-driven photocatalyst while Ag is used as electron-transfer system, and this nanojunction system exhibited high photocatalytic activity in disinfection of *E.coli* K-12 and degradation of azo dye and colorless pollutant pentachlorophenol.[54-55] To date, 3D mesoporous AgBr/Bi_2WO_6 heterojunction has never been constructed. Silver bromide (AgBr) with a narrow band gap (~2.6 eV), is an important photosensitive semiconductor. Under solar irradiation, AgBr can absorb photons to generate electrons and holes. Thus AgBr can be used as potential photocatalyst. But the photoinduced electrons will combine with interstitial Ag^+ ions to form an Ag^0 cluster, which leads to photodecomposition of AgBr. So, the instability of pure AgBr is a obstacle in practical photocatalytic application. The well-fabricated Bi_2WO_6-based p-n heterojunction could restrict the recombination of charge carriers and enhance the quantum yield. The photo-induced electron can transfer from p-type semiconductor to Bi_2WO_6, which favors the charge separation and also improve the visible-light photocatalytic activity of heterojunction. To this end, we intend to design heterojunction by coupling Bi_2WO_6 with a p-type narrow-band-gap semiconductor with matched potentials. In current work, we synthesized the uniform hierarchical mesopouous 3D Bi_2WO_6 architectures with diameter of 2~4 μm, and furthermore, monodispersed AgBr nanodots was deposited on the surface of Bi_2WO_6 followed by employing a facile precipitation-deposition process because of its relative simplicity and its versatility in the preparation of heterojunction nanostructure of photocatalyst. As-prepared AgBr/Bi_2WO_6 heterojunctions were subsequently characterized by a number of techniques including XRD, SEM, TEM, HRTEM as well as EDS and XPS. The methylene blue (MB) and phenol were chosen as the model pollutant to evaluate the photocatalytic activity of the samples under visible light irradiation. The experimental results demonstrated that AgBr nanodots loaded hierarchical Bi_2WO_6 nanoastructures exhibited significantly enhanced photocatalytic activity in photo-degradation of MB dye and phenol, highly stability and easy to be recycled. Furthermore, the mechanism of enhanced photocatalytic activity for hierarchical AgBr/Bi_2WO_6 p-n nanojunction was also discussed based on the calculated energy positions of AgBr and Bi_2WO_6.

2 Experimental Section

2.1 Sample Preparation.

All of the chemicals were analytical grade and used without further treatment. Bi_2WO_6 architectures were synthesized by hydrothermal reaction under autogenerated pressure. In a typical procedure, 0.4 g (1.0 mmol) $Bi(NO_3)_3$ was first dissolved in 20 mL of nitric solution (0.4 $mol\cdot L^{-1}$), and then 10 mL of $(NH_4)_{10}W_{12}O_{41}$ solution with concentration of 0.0082 $mol\cdot L^{-1}$ was added drop-wise to the above solution under vigorous magnetic stirring at room temperature. Under stirring, the diluted NaOH and HNO_3 (4 $mol\cdot L^{-1}$) were used to adjust the pH value to 1. After being magnetic stirred at room temperature for 2 h, the resulting precursor suspension was transferred into a 50 mL Teflon-lined autoclave. The autoclave was then sealed and maintained at 190 □ for 2 h. Subsequently, the autoclave was cooled to room temperature naturally. After filtration, the yellowish white precipitate was collected and washed with distilled water and absolute ethanol several times, then dried under vacuum at 80 □ for 4 h.

AgBr nanodots loading Bi_2WO_6 was prepared by a precipitation-deposition process. The obtained Bi_2WO_6 (1 mmol) was dispersed in water by magnetic stirring, and then appropriate amounts of $Ag(NH_3)_2^+$ was added. Then the suspension was irradiated for 3 h under stirring at ambient temperature, and certain amount of excessed KBr aqueous solution was dropwised to the mixture solution. After stirring for 2 h, the obtained AgBr-loaded Bi_2WO_6 was washed with water to remove the excessed K^+ and Br^- and dried in a vacuum at 80 ^oC for 2 h. To investigate the effects of contents of AgBr on the photocatalytic activity of Bi_2WO_6, the added contents of $Ag(NH_2)_2^+$ varied from 0.5% to 10.0%, so the resulted samples were denoted as 0.5, 1.0, 2.0, 5.0 and 10.0at%AgBr/Bi_2WO_6, respectively.

According to the literature,[56] $TiO_{2-x}N_x$, known for it good photocatalytic activity in decomposition of pollutants under visible-light irradiation, was also prepared as a reference to compare the photocatalytic activity with our sample.

2.2 Characterization.

Powder X-ray diffraction (XRD) was carried out with a Shimadzu XRD-7000 X-ray diffractometer using Cu Kα radiation (λ = 0.15418 nm) at a scanning rate of 2°/min in the 2θ range from 20° to 80°. The accelerating voltage and the applied current were 40 kV and 30 mA, respectively. The Brunauer-Emmett-Teller (BET) specific surface area (S_{BET}) of the samples was

measured by nitrogen adsorption in an ASAP2010 from Micromeritics Instrument Corporation. X-ray photoelectron spectroscope (XPS) images were recorded on a PHI-5400 X-ray photoelectron spectrometer. The field emission scanning electron microscope (FE-SEM) images were taken on a JSM-6700F scanning electron microscope. High-resolution transmission electron (HR-TEM) images and selected area electron diffraction (SAED) patterns were recorded on a JEM-2100 electron microscope at an accelerating voltage of 200 kV. The UV-Vis diffuse reflectance spectra(UV-Vis-DRS) of the samples were obtained using Shimadzu UV-2550 UV-Vis spectrophotometer. $BaSO_4$ was used as a reflectance standard.

2.3 Photocatalytic experiment.

The evaluation of photocatalytic performance of samples for photocatalytic decolorization of MB aqueous solution was performed as follows: A 500 W Xe-arc lamp was used as the visible-light source with a cutoff filter to cut off the light below 420 nm. The suspensions containing 200 mg of photocatalyst and 250 mL fresh aqueous solution of MB or phenol (10 $mg \cdot L^{-1}$) were continuously magnetically stirred in the dark for 1 h to establish an adsorption/desorption equilibrium of MB solution. After this period of time, the light source was turned on. During the reaction, 5 mL of samples were taken at given time intervals and then separated Bi_2WO_6 photocatalysts through centrifugation(Fig. S1). For MB concentration detection, the supernatant solution was decanted and the absorbance of MB was determined through its maximum absorption band using a Shimadzu 2550 UV-visible spectrophotometer and the absorption peak at 553 nm was monitored. The concentration of phenol was determined by using 4-aminoantiphytine spectrophotometic method (Chinese HJ 503-2009). Total organic carbon analyzer (Vario TOC, Elemental, Germany) was employed for mineralization degree analysis of MB and phenol solutions.

3. Results and discussion

3.1 XRD and XPS.

The phase structure, crystallinity and purity of as-obtained product were examined by XRD measurement. The lattice parameters, crystallite size and BET specific surface area for samples are summarized in Table 1. The BET surface areas of pure Bi_2WO_6 and AgBr loaded Bi_2WO_6 are about 47.6~ 46.0 m^2/g, respectively. Their XRD patterns are compared in Fig. 2, and the diffraction peaks can be categorized into two sets: one set peaks at 2θ of 28.3°, 32.8°, 32.9°, 47.0°, 47.1°, 55.8°, 58.5°, 68.7°, 75.9° and 78.5° can be perfectly indexed to an orthorhombic Bi_2WO_6 (JCPD file no.39-0256), corresponding to the indices of (131), (200), (002) , (260), (202), (331), (262), (400), (103) and (204) planes, respectively, while another set peaks agree well with face-centered cubic AgBr corresponding to JCPDS files no. 6-0438(Figs.1b~f). No peaks of other impurities are detected, indicating satisfactory purity of the products. After refinement, the lattice parameters of the samples are obtained (Table 1). It is clear that there is neglectable change in lattice parameters between Bi_2WO_6 and AgBr loaded Bi_2WO_6.

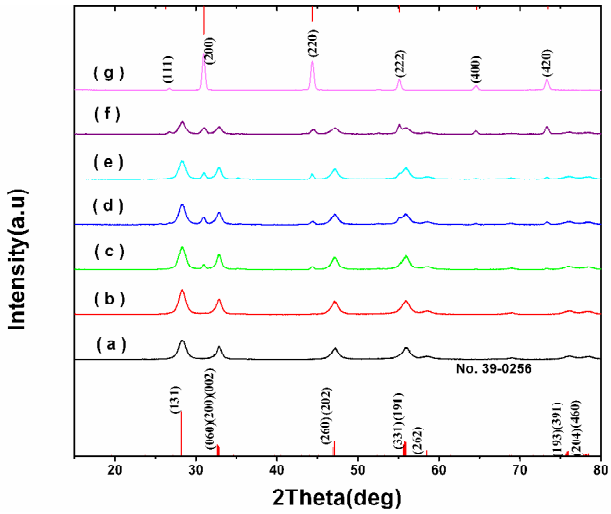

Fig. 1 XRD patterns of as-synthesized samples. (a)pure Bi_2WO_6 and AgBr-Bi_2WO_6 compsite photocatalyst with different AgBr content: (b)0.5at%, (c)1.0at%, (d)2.0at%, (e)5.0at%, (f)10.0at%, (g)pure AgBr.

Table 1 The lattice parameters and BET specific surface area for samples.

Sample	BET(m^2/g)	Lattice parameters		
		a(Å)	*b*(Å)	*c*(Å)
Pure-Bi_2WO_6	47.6	5.458(2)	5.431(8)	16.403(4)
0.5at%AgBr-Bi_2WO_6	47.8	5.456(1)	5.432(8)	16.402(8)
1.0at%AgBr-Bi_2WO_6	47.6	5.457(2)	5.432(8)	16.403(4)
2.0at%AgBr-Bi_2WO_6	46.8	5.458(2)	5.434(6)	16.403(3)
5.0at%AgBr-Bi_2WO_6	46.8	5.459(2)	5.432(4)	16.403(5)
10.0at%AgBr-Bi_2WO_6	46.0	5.456(2)	5.432(8)	16.403(6)

Further evidence for the chemical composition and oxidation states of the as-prepared AgBr loaded Bi_2WO_6 architectures was obtained by the X-ray photoelectron spectroscopy (XPS) technique (Fig. 2). Figs. 2b-2e shows the high-resolution spectra of the Bi 4f, W 4f, O 1s, Ag 3d and Br 3d regions, respectively. In Fig. 2b, two peaks at 159.4 eV and 162 eVare attributed to Bi $4f_{7/2}$ and Bi $4f_{5/2}$ of Bi^{3+} in 2.0at%AgBr/Bi_2WO_6. Peak at 37.5 and 35.2 eV, as shown in Fig. 2c, corresponding to W $^4F_{5/2}$ and W $^4F_{7/2}$, respectively, can be assigned to a W^{6+} oxidation state.[57] As shown in Fig. 2d, the asymmetric XPS of O 1s may be fitted into two kinds of chemical states: crystal lattice oxygen and adsorbed oxygen.[58-60] Fig. 2e gives the high-resolution XPS spectrum of Ag3d. The $Ag3d_{3/2}$ and $Ag3d_{5/2}$ peaks are identified at 367.96, 373.83 eV, respectively, suggesting the presence of Ag^+.[61] Moreover, in Fig. 2e the peak of Br 3d at 69.07 eV is due to the crystal lattice of Br^- in AgBr.[62] Therefore, with combination of XPS and XRD investigation, the results confirmed that there were both Bi_2WO_6 and AgBr species in the 2.0at%AgBr/Bi_2WO_6 sample. Furthermore, peak areas were determined for the quantitative elemental analysis of Bi, W, O, Ag and Br in 2.0at%AgBr/Bi_2WO_6 architectures, and the atomic ratio of Bi: W: O: Ag is 2:1:6.01:0.02.

3.2 Morphology and structure.

The morphology of as-synthesized samples was examined by FE-SEM, as shown in Fig.3. It can be seen that pure-Bi_2WO_6 exhibits an uniform three-dimensional (3D) nest-like architectures with scales of 2~4 μm(Fig. 3a). Interestingly, the nest-like Bi_2WO_6 3D architectures consist of many secondary nanoplates with thickness of 10~20 nm. When AgBr was deposited on the surface of 3D Bi_2WO_6 architectures *via* a facile precipitation-deposition process (Figs.3b-3e), the resulted AgBr/Bi_2WO_6 composite sample exhibits the similar morphology and size to that of pure Bi_2WO_6. With the increasing AgBr content, the more AgBr nanoparticles was dispersed on the surface of Bi_2WO_6. Obviously, the coexistence of AgBr and Bi_2WO_6 did not significantly affect their morphology. Further information about the AgBr/Bi_2WO_6 nanoarchitectures was obtained from TEM, and HR-TEM images (Figs.3e~3f). It can be seen that the 3D Bi_2WO_6 architectures are built up by Bi_2WO_6 nanoplates with thickness of 10-20 nm (Fig.3f). The corresponding selected area electron diffraction (SAED) pattern (upper part of insert picture in Fig.3f) reveals the well-aligned clear diffraction sports that can be indexed to the orthorhombic structure of Bi_2WO_6. The single crystalline nature and parameters of nanoplates were also confirmed by HR-TEM (lower part of insert picture in Fig. 3f). The spacing of the lattice fringes was found to be about 0.315 nm, as shown in Fig.3f, which is in good agreement with the *d*-spacing of (131) planes of orthorhombic Bi_2WO_6. Furthermore, the locations of AgBr quantum dots on the surface of Bi_2WO_6 nanoplate are pointed by arrows in TEM image (left of Fig. 3f). It reveals that some small spherical heteroparticles with size of about 10 nm covered over the surface of Bi_2WO_6 architectures, indicating that AgBr nanodots were

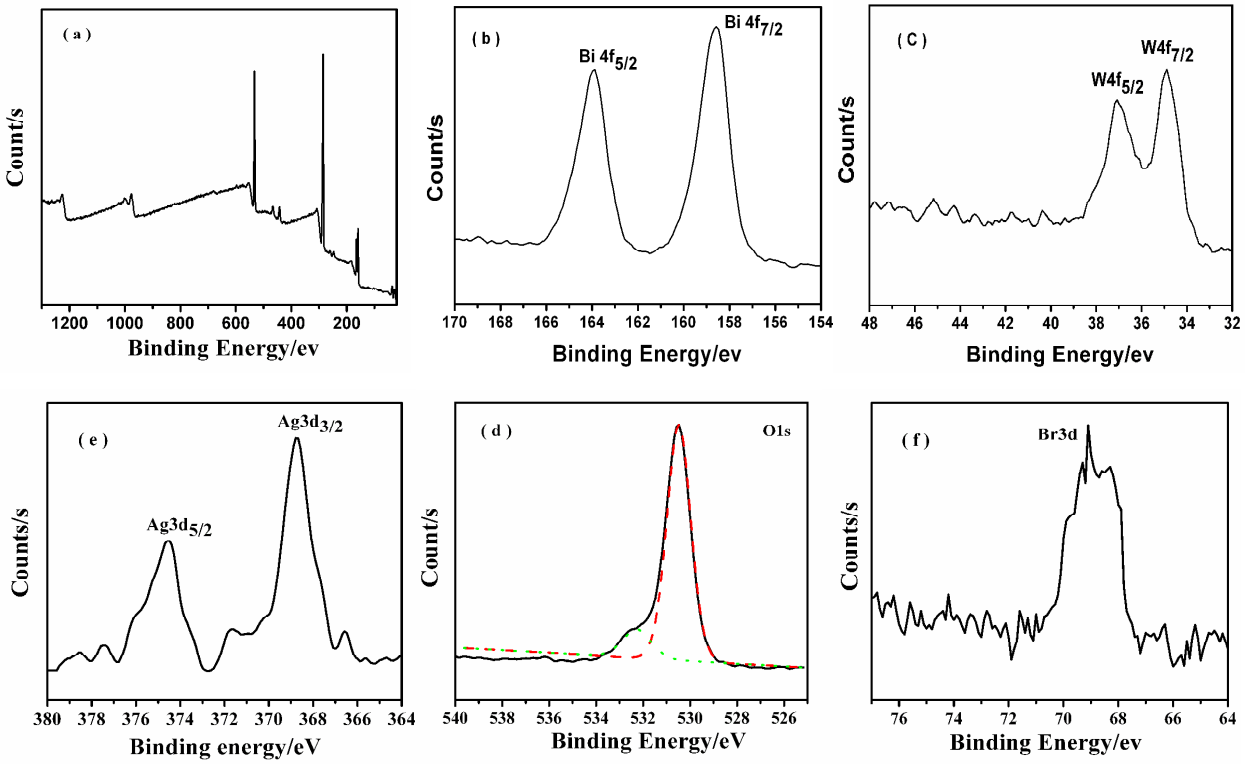

Fig. 2 XPS spectra of 2.0at%AgBr/Bi_2WO_6. (a) The survey spectra, and the high resolution XPS spectra of the sample: (b) Bi4f ; (c) W4f ; (d)O1s; (e) Ag3d; (f) Br3d.

highly dispersed on the surface of Bi_2WO_6 nanoarchitectures and formed the heterojunction structure, which is well consistent with the XRD and XPS results. Although the SEM, TEM and HRTEM did not provide clear information about the composition in the sample, the EDS analysis demonstrated that Ag and Br elements existed in the sample. The molar ratio of AgBr to Bi_2WO_6 obtained in the powder was also close to the theoretical calculated value of AgBr/Bi_2WO_6 (insert table in Fig.3g).The EDS patterns of the 2.0at.%AgBr/Bi_2WO_6 heterojunction indicated that, besides Bi, W and O peaks coming form the Bi_2WO_6,, the Ag and Br diffraction peaks corresponding to AgBr were also observed, further confirming that the sample was composed of Bi_2WO_6 and AgBr. According to EDS spectrum, the AgBr content of 2.0at%AgBr/Bi_2WO_6 sample was determined to be 1.98%. Therefore, with the combination of the XRD、XPS、SEM、EDS and TEM investigation, the results confirmed that there were both Bi_2WO_6 and AgBr species in the heterojunction structure.

In order to investigate the porous structure of the as-synthesized Bi_2WO_6, N_2 adsorption/desorption isotherms and Barrett-Joyner-Halenda (BJH) pore size distribution analysis were performed. As shown in Fig. S2, the nitrogen adsorption and desorption isotherms can be categorized as type IV isotherm with a hysteresis loop observed in the relative (P/P_0) range of 0.4-1.0, which implies the presence of mesoporous in the size of 2-50 nm.[32] The hysteresis loop shifts to a higher pressure on approaching $P/P_0 \approx 1$, which suggests that macrospores are also present. This is also confirmed by the corresponding pore-size distribution that shows two peaks for mesopores along with macrospores up to 100 nm in size (insert picture in supporting information Fig. S2). These pores presumably arise from the spaces among the nanoplates within the nest-like 3D Bi_2WO_6 architecture. The 3D nest-like Bi_2WO_6 architectures possess small mesoporous of ca.8.5 nm and large mesoporous with a peak at about 45 nm. As revealed by FE-SEM observation, the smaller pores may be generated during the crystal growth process, whereas the larger pores can be attributed to the space between the intercrossed Bi_2WO_6 nanoplates.[63] The BET surface area of nest-like 3D Bi_2WO_6 architecture was calculated from N_2 isotherms is 47.6 $m^2 \cdot g^{-1}$. The single-point total volume of pores at P/P_0 = 0.991 is 0.452 $cm^3 \cdot g^{-1}$. The porous structure and the large BET surface area may endow the as-prepared 3D nest-like architecture Bi_2WO_6 architecture with novel application. As shown in Table 2, the BET surface area of of AgBr/Bi_2WO_6 architecture don't exhibit obvious change.

3.3. UV-Vis-DRS analysis.

Fig. 4 shows the typical UV-Vis-DRS spectra of pure Bi_2WO_6 and AgBr/Bi_2WO_6 heterojunction with different AgBr content. Pure Bi_2WO_6 presents the photo-absorption properties from the UV light region to visible light about 450 nm due to the intrinsic band-gap transition. The absorption spectra of AgBr/Bi_2WO_6 heterojunction are obviously different from that of pure Bi_2WO_6. When AgBr loaded on the surface of Bi_2WO_6, the absorption of AgBr/Bi_2WO_6 heterojunction within visible light range enhanced apparently and a redshift appeared upon the content of AgBr increased. The redshift of the absorption wavelength indicated that the photocatalyst could absorb more photons. Therefore, the redshift in the absorption band could be favorable for photocatalytic reaction. Aside from the photoabsorption from Bi_2WO_6, the AgBr/Bi_2WO_6 heterojunction displays another wide absorption around 450~700 nm peaked at about 560 nm, corresponding to the indirect band-gap of AgBr.[54,60] Comparison to the adsorption peak position of pure-AgBr, the adsorption peak of AgBr/Bi_2WO_6 shows a obvious "blue-shift". These results were contributed to the interaction between AgBr and Bi_2WO_6 in the samples.

3.4. Photocatalytic activity.

Methyl blue (MB), a chemically stable molecule, was selected as probe molecule to assess reactivity of the samples. As shown in Fig. 5a, without catalyst the concentration of MB remains unchanged even after 1 h of visible-light irradiations. The photocatalytic performances of the AgBr/Bi_2WO_6 heterojunction with different AgBr contents were determined by comparing the degradation efficiency of MB (Fig.5). By analyzing the change of concentration of MB solution vs illumination time (Fig. 5a), the result well obeys the pseudo-first-order kinetics model, i.e. $\ln(C_t/C_0) = -kt$, where C_t and C_0 are the concentration of MB at time t and 0, respectively, and k is the pseudo-first-order rate constant. The rate constant, k, of MB photodegradation was derived from the $\ln(C_t/C_0) \sim t$ plots (Fig. 6) and listed in table 2. It was found that when a 500 W Xe-arc lamp was used as the visible light source with a cutoff filter to cut off the light below 420 nm, all of the 3D AgBr/Bi_2WO_6 heterojunction architectures exhibited better photocatalytic activity for MB degradation than the pure-Bi_2WO_6. It could be clearly seen that the photocatalytic degradation of MB was 33.5%, 84.6%, and almost 100.0% for pure AgBr, pure Bi_2WO_6 and 2.0at%AgBr/Bi_2WO_6 heterojunction after illumination for 30.0 min, respectively, which indicated that MB could be degraded more efficiently by AgBr/Bi_2WO_6 heterojunction than pure AgBr and Bi_2WO_6.

Fig. 5b shows the temporal evolution of MB solution over 2.0at%AgBr/Bi_2WO_6 heterojunction photocatalyst. With the increasing of irradiation time and in the presence of 2.0at%AgBr/Bi_2WO_6 suspension, the intensity of the absorption peak at 663 nm decreased quickly with 30 min, which indicated that 2.0at%AgBr/Bi_2WO_6 heterojunction exhibited high photocatalytic activity. In addition, it also found that the photocatalytic activity of AgBr/Bi_2WO_6 with AgBr content higher than 2.0at% were lower that that of 2.0at%AgBr/Bi_2WO_6

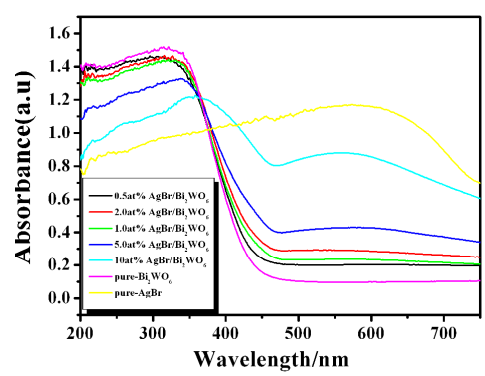

Fig. 4 UV-Vis-DRS spectra of as-synthesized samples. (comparison of pure-Bi_2WO_6, AgBr and AgBr/Bi_2WO_6 heterojunction photocatalyst with different molar ratio).

under visible light irradiation.

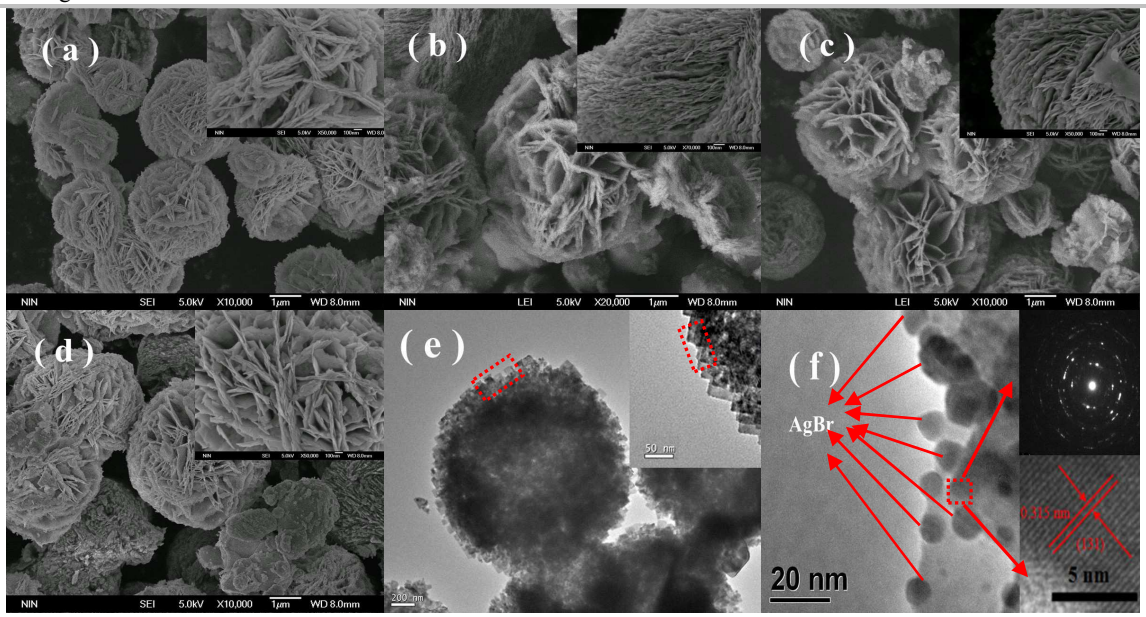

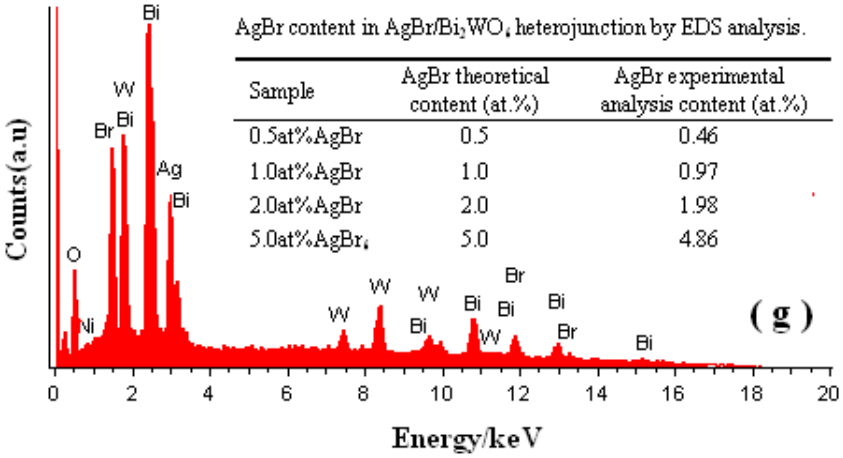

AgBr content in AgBr/Bi_2WO_6 heterojunction by EDS analysis.

Sample	AgBr theoretical content (at.%)	AgBr experimental analysis content (at.%)
0.5at%AgBr	0.5	0.46
1.0at%AgBr	1.0	0.97
2.0at%AgBr	2.0	1.98
5.0at%AgBr	5.0	4.86

Fig.3 FE-SEM images of samples. (a) pure- Bi_2WO_6 and AgBr/Bi_2WO_6 campsite photocatalysts with different AgBr content: (b)1.0at%, (c)2.0at%, (d)5.0at%; (e~f)TEM, HR-TEM and SAED of 2.0at%AgBr/Bi_2WO_6 heterojunction; (g) EDS spectrum of 2.0at.%AgBr/Bi_2WO_6 sample according to (d), the insert table in Fig. 3g shows the AgBr content in AgBr/Bi_2WO_6 by EDS analysis.

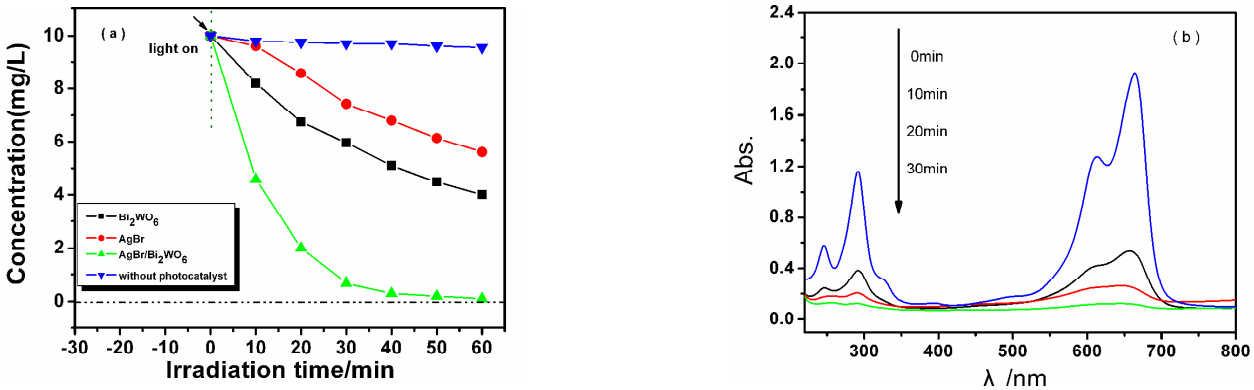

Fig. 5 Photocatalytic degradation efficiency of MB by different catalysts. (a) Photocatalytic activity comparison of different photocatalysts; (b) changes of UV -Vis absorption spectra of MB by 2.0at%AgBr/Bi_2WO_6 heterojunction structure.

Table 2 Pseudo-first-order rate for MB photocatalytic oxidation under different photocatalysts.

Sample	The first order kinetic constant and coefficient	
	k (min^{-1})	R^2
pure-Bi_2WO_6	0.0151	0.9902
0.5at%AgBr-Bi_2WO_6	0.0175	0.9862
1.0at%AgBr-Bi_2WO_6	0.0354	0.9886
2.0at%AgBr-Bi_2WO_6	0.0785	0.9883
5.0at%AgBr-Bi_2WO_6	0.0464	0.9986
10.0at%AgBr-Bi_2WO_6	0.0165	0.9896

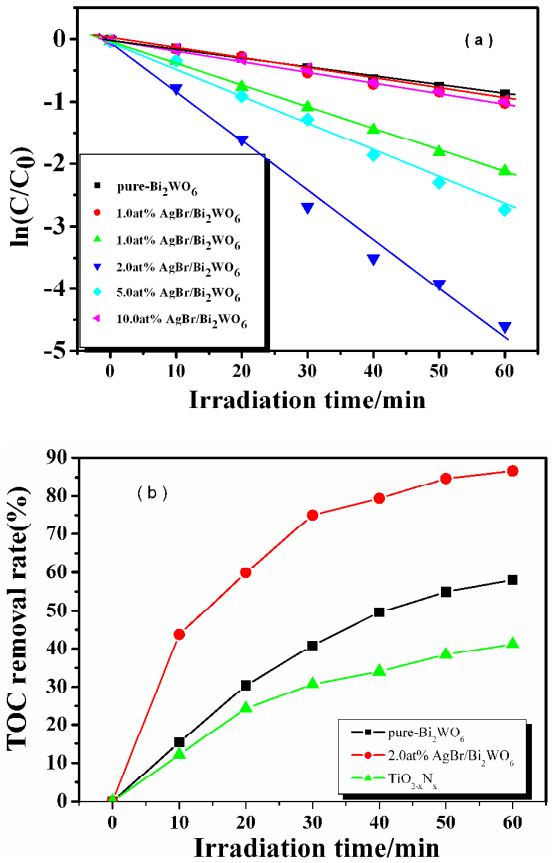

Fig. 6 (a) Photocatalytic degradation efficiency of MB by different catalysts. (b) TOC changes during the course of of MB photodegradation in the present of pure-Bi_2WO_6, 2.0at%AgBr/Bi_2WO_6 heterojunction structure and $TiO_{2-x}N_x$, respectively.

Fig.6a and Table 2 show the rate constant values (k) of AgBr/Bi_2WO_6 series catalysts with different AgBr content for degradation of MB solution. Interestingly, among such heterojunctions, 2.0at%AgBr/Bi_2WO_6 heterojunctions exhibited the highest photocatalytic activity with nearly 100% MB discoloration in the initial 30 min irradiation. The apparent rate constant k is 0.0785 min^{-1} for 2.0at%AgBr/Bi_2WO_6. For comparison, the MB photodegrdation by $TiO_{2-x}N_x$ and pure-Bi_2WO_6 were also performed. The results are shown in Fig.S3. One can see that the degradation of MB over 2.0at%AgBr/Bi_2WO_6 was more rapid than that in case of $TiO_{2-x}N_x$ and pure-Bi_2WO_6.

In order to further investigate the activity of 2.0at %AgBr/Bi_2WO_6, the TOC experiment was performed (Fig.6b). The result shows that the mineralization yield of 2.0at %AgBr/Bi_2WO_6 reaches a value of 75.6% after 30 min of irradiation, while that of pure-Bi_2WO_6 and $TiO_{2-x}N_x$ is 40.8% and 31.6.3% after 30 min irradiation. The rate of TOC reduction of 2.0at %AgBr/Bi_2WO_6 is slower than that of the degradation of dye, which is nearly 100% discoloration for MB in 30 min as shown Fig.5a. It is well-known that the mineralization of the dye goes through two steps: the ring cleavage and subsequently the oxidation of the fragments. In our experiment, the TOC removal rate of 2.0at%AgBr/Bi_2WO_6 exhibited two different behaviors before and after 30 min of irradiation, respectively. These results confirm that that MB is first ring cleavage and then converted into CO_2. The loss of TOC via mineralization can be lowered more than removed amount of organic pollutants because these parent molecules are decomposed to smaller organic intermediates, and further degradation of these intermediates to CO_2 and H_2O may take place slowly.[54]

Photocatalytic activities of AgBr/Bi_2WO_6 can be further demonstrated by the degradation of some other organic compound,

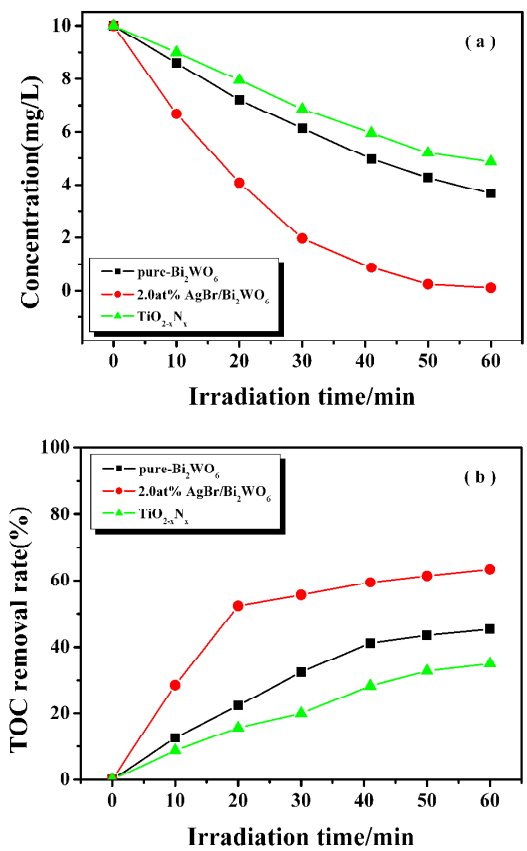

Fig. 7 (a) Photocatalytic degradation efficiency of phenol by different catalysts. Photocatalytic activity comparison of different photocatalysts; (b) TOC changes during the course of of MB photodegradation in the present of pure-Bi_2WO_6, 2.0at%AgBr/Bi_2WO_6 heterojunction structure and $TiO_{2-x}N_x$, respectively.

such as phenol that has no light absorption characteristics in the visible spectral region. Upon visible-light irradiation, phoenol is degraded more efficiently by 2.0at%AgBr/Bi_2WO_6 nanojunction system than by any other photocatalyst (Fig. 7a), such as Bi_2WO_6 and $TiO_{2-x}N_x$. In addtion, we also detected the change of TOC induced by 2.0at%AgBr/Bi_2WO_6 nanojunction, pure-Bi_2WO_6 and $TiO_{2-x}N_x$ under the same identical condition. It is clear that that TOC of the solution continuously decreases, indicating that phenol steadily mineralized by photocatalysts under visible-light irradiation. The mineralization of phenol within 60 min induced by 2.0at%AgBr/Bi_2WO_6 reaches 63.4% as shown in Fig.7b, which is much higher than that of pure-Bi_2WO_6 and $TiO_{2-x}N_x$. This further confirms that the photocatalytic performance of AgBr/Bi_2WO_6 nanojunction is superior to that of pure-Bi_2WO_6 and $TiO_{2-x}N_x$.

For comparision, a summary of literatures using photocatalyst for degradation of methylmene bule is shown in Table S1. It can be seen that various kind of photocatalysts have been employed to photograde methylene bule, and 2.0at%AgBr/Bi_2WO_6 heterojunction photocatalyst exhibits higher photocatalytic activity than that of the reported photocatalysts.

The photocatalytic activities of the AgBr/Bi_2WO_6 enhanced remarkably with increasing AgBr content, but higher AgBr loading content, the photocatalytic activity decreased, suggesting that the optimal AgBr content in AgBr/Bi_2WO_6 existed when the molar ratio was 2.0at%. The same phenomenon also reported in other systems, such as AgBr/$BiPO_4$, [62] AgBr/WO_3, [64] SnO_2/TiO_2, [65] *etc*. The optimum content of AgBr in the heterojunction can be related to the recombination rate of photogenerated electrons and holes. According to literatures reported,[64-66] the space charge region potential for the efficient separation of electron-hole must be certain. When AgBr content was above its optimal vale, the space charge region might become very narrow and the penetration depth of Bi_2WO_6 exceeds the space charge layer, so the recombination of the photogenerated electron-hole pairs in semiconductors become easier. On the other hand, when AgBr content was below its optimal value, the photocatalytic activity was low because fewer electron and hole trapping carriers could be detrimental to the separation of electron-hole pairs. Besides that, the size of AgBr on the surface of Bi_2WO_6 was also investigated (Fig. S4). It clearly indicated that all the samples prepared with different AgBr content exhibited the similar size of ~10 nm. According to the quantum size effect, when the particle size of semiconductor is less than 100 nm, the absorption edge will show a "blue-shift". The similar size of AgBr particles means the similar quantum size effect. Combined with Fig.4, we can see that with the deposition amount of AgBr increasing, the absorption edge of AgBr/Bi_2WO_6 shown a obvious "red-shift". These results were contributed to the interaction between AgBr and Bi_2WO_6 in the samples. So we can believe that it is the content rather than the size of AgBr affect the photocatalytic activities of AgBr decorated mesoporous Bi_2WO_6, and more research should be gone deep in.

3.5 Photocatalytic mechanism. The enhanced photocatalytic activity of the AgBr/Bi_2WO_6 heterojunction architecture can be explained by improvement of the charge separation due to the loaded of AgBr. When AgBr content is lower than 2.0at%, the photocatalytic activity Bi_2WO_6 architecture is enhanced with the increase of AgBr content. When the content of loaded AgBr is higher than 2.0at%, the photocatalytic activity of AgBr/Bi_2WO_6 heterojunction architecture decreased with the increase of AgBr content because the higher AgBr deposits conversely behave as recombinant centers, encouraging the recombination of charge carriers.[62]

It is known that the activity of photocatalyst mostly depended on the light energy utilization ration and quantum efficiency, which is closely related to the efficiency of the photogenerated electron-hole separation and the diffusion from the inner regions to the surface of the grains.[67] To approach the mechansim of enhanced photocatalytic activity of as-obtained AgBr/Bi_2WO_6 heterojunction, the relative band positions of two semiconductor were investigated. In AgBr/Bi_2WO_6, Bi_2WO_6 is typical n-type semiconductor and AgBr is p-type semiconductor. When AgBr nanodots were coupled on the surface of Bi_2WO_6, novel p-n nanojunction would be formed. According to literatures,[62, 67-69] at the thermodynamic equilibrium of p-n heterojunction, there is an internal field with direction from n-type to p-type.[62, 68] The p-n composite heterojunction decreases the recombination rate of photogenerated electrons and holes via the speical internal electric field. As depicted in Fig.8, while AgBr/Bi_2WO_6 photocatalyst is being irradiated, both Bi_2WO_6 and AgBr can be easily excited and corresponding photoinduced electrons and holes are generated. CB-electrons of AgBr could be easily injected into CB of Bi_2WO_6 because the CB of Bi_2WO_6 is positive than that of the loaded AgBr QDs and the intimate contact between the two semiconductors. Simultaneously, photoinduced holes on the VB of Bi_2WO_6 can be transferred to that of AgBr.[67-68] In such way, photoinduced electrons and holes can be efficiently separated and the recombination of electron-hole pairs can be suppressed efficiently. In the present study, PL spectrum was employed to explain this process. Since PL emission mainly results from the recombination of excited electrons and holes, PL emission spectra are useful in determining the efficiency of charge carrier trapping, migration and transfer, and helpful in understanding the fate of electron-hole pairs in semiconductor particles.[45,72-74] Its recombination efficiency might be reduced because of a fraction of holes in the Bi_2WO_6 transfer to AgBr. A low PL intensity implies a low recombination rate of the electron-hole under light irradiation.[71] Fig. 9 shows the comparison of PL spectra of as-prepared pure-Bi_2WO_6 and AgBr/Bi_2WO_6. When the excitation wavelength was 300 nm, Bi_2WO_6 has a broad blue-green emission peak at 430-530 nm.[31, 73] The PL spectrum of as-prepared Bi_2WO_6 revealed that four peaks appeared at 423, 460, 475 and 535 nm. The strongest blue emitting peaks at ca. 475 nm is attributed to the intrinsic luminescence of Bi_2WO_6, which originates from the photoinduced electron transfer transitions between the hybrid of Bi6s and O_{2p}(VB) to the empty W_{5d} orbital(CB) in WO_6^{2-} complex.[75] The blue emission peak centered at 423 nm is attributed to the intrinsic transition of Bi^{3+} ions from $^3P_1$(6s6p) excited state to the $^1S_0$ ($6S^2$) ground state.[75-77] The emitting peak at 535 nm (green) is ascribed to the defects of metal atoms and oxygen vacancies during the crystal growing process,[78-79] which is become many defect centers and thus affect the optical properties of Bi_2WO_6. It was found that the PL emission spectra of the pure-Bi_2WO_6 and AgBr/Bi_2WO_6 showed the main peaks at similar positions but with different intensities. The PL intensity of AgBr/Bi_2WO_6 is lower than that of pure Bi_2WO_6, which clearly indicates that the recombination of photo-generated charge carrier

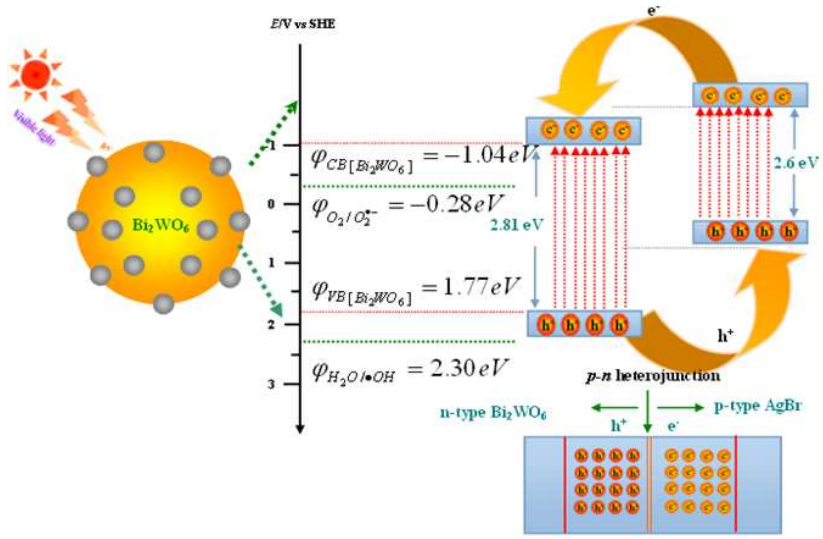

Fig. 8 The potential of valence and conduction band for AgBr and Bi_2WO_6 to illustrate the photocatalytic activity enhancement mechanism of AgBr/Bi_2WO_6 p-n heterojunction.

between the CB-Bi_2WO_6 (the empty W5d orbital) to the VB-Bi_2WO_6 (the hybrid of Bi6s and O2p) is greatly inhibited in the semiconductors heterojunctions.[31, 72-74] In order to further insight into the active species of AgBr/Bi_2WO_6 photocatalyst, we also display the potential vs SHE of hydroxyl radicals and superoxide radical anions (Fig.6), which display a potential vs SHE of 2.3 eV and -0.28 eV, respectively.[11, 66, 83] As depicted in Fig.8, the standard redox potentials of positive holes photogenerated in the valence band of both Bi_2WO_6 and AgBr are more negative than that of of •OH/H_2O, while the potentials of CB-electrons of Bi_2WO_6 and AgBr are more negative than that of O_2/O_2•$^-$. Consequently, depending on the relative band edge position, AgBr/Bi_2WO_6 heterojunction may generate O_2•$^-$ radicals, and it is not likely to produce the •OH. According to previous studies,[79-80] the degradation of dye involves two possible mechanism. The first is true photocatalysis process, which causes the formation of the hole-electron pairs. Thus, oxidation reactions can occur to provide •OH radicals, which are non-selective strong oxidizing agents that react with the dye molecule causing its degradation and subsequent mineralization. Another possible mechanism is through a photosensitization process. In this case, dye molecule absorbs visible light so that it reaches an excited state. The electron of excited state is directly injected into the conduction band (CB) of semiconductor. The CB delocalizes the electrons through series of reduction reactions, such as formation of O_2•$^-$. During the photocatalytic process of AgBr/Bi_2WO_6 heterojunction, O_2•$^-$ may be the main active species.

To further confirmed the possible reaction mechanism for photodegradation of MB over AgBr//Bi_2WO_6, We have performed a series of controlled experiments under visible irradiation, as shown in Fig.S5. The photocatalytic reactivity in the presence of dissolved oxygen should be compared with the anoxic reactivity. MB photocatalytic degradation could be carried out with continuous N_2 sparging in a stricter anoxic. The reaction performed in nitrogen atmosphere showed lower degradation of MB, indicating that molecular oxygen is the crucial to the reaction. In addition, molecular oxygen is a well-known acceptor of photogenerated electrons, thereby generating the superoxide radical species(O_2•$^-$) and preventing the recombination of electron-hole pairs. When benzoquinone(BQ), a scavenger for O_2•- radicals, is added to the reaction, the photodegradation of MB is decreased apparently. Also, isopropyl alcohaol was employed as a radical scavenger for •OH, and KI a hole scavenger. As shown in Fig.S5, after reaction of 60 min, the photodegradation process was decelerated after KI was added and the degradation rate of greatly decreased from 99.2% to 80.8%, while the degradation rate of 96.8% was obtained after isopropyl alchoal was added, suggestiong that •OH radicals are not involved in the photocatalytic oxidation of MB. Accroding to literatures,[81-83] the standard redox potential of positive holes photogenerated in the valence band of Bi_2WO_6 is more negative than that of •OH/H_2O, suggesting that hole on the surface of Bi_2WO_6 could

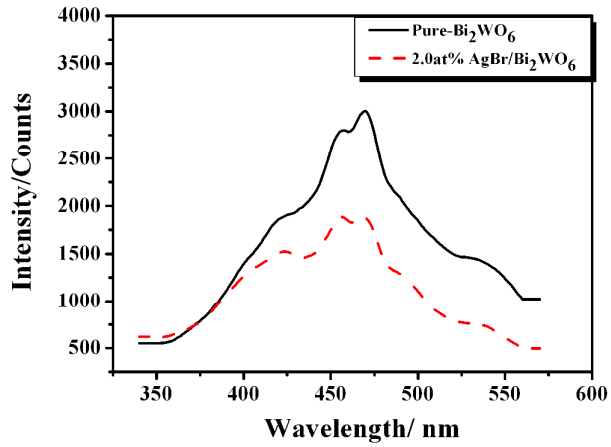

Fig. 9 The room temperature photoluminescence (PL) spectrum of Bi_2WO_6 (a), and 2.0at%AgBr/Bi_2WO_6 nanoarchitecture ($\lambda_{excitation}$= 300 nm)

not react with OH^-/H_2O to form "non-selective" •OH radicals in heterogeneous photocatalytic oxidation. The above results clearly indicate that the degradation of MB over AgBr//Bi_2WO_6 is primarily driven by photogenerated holes and $O_2•^-$, and •OH is not responsible for the degradation of MB.

It is worth noting that the generation of $O_2•^-$ could be via two processes. On one hand, dye is excited by visible light to form excited state (dye*). The excited state then injects electrons into the CB of catalyst via electron transfer to generate a conduction that is scavenged by the O_2 on the surface of the catalyst to form $O_2•^-$. Once the dispersion discolors completely, the formation of $O_2•^-$ by this route will terminate automatically. Because the redox potential of MB is more positive (0.532 eV) than that of $O_2•^-$, the excited stage(MB*) may not transfer electrons to the the CB of catalyst to form $O_2•^-$. On the other hand, when AgBr/Bi_2WO_6 heterojunction photocatalyst absorb light, the photogenerated electrons could react directly with O_2 adsorbed on the surface of AgBr/Bi_2WO_6 heterojunction photocatalyst to form O_2•-. The O_2•- active species is produced through the whole photochemical process.

Based on our experimental results and the discussions above, the mechanism of photocatalytic degradation of MB on the AgBr/Bi_2WO_6 heterojunctions may be proposed, as described in the equations ①~⑤. Under the visible-light irradiation, photo-holes and electrons were generated in VB and CB of catalyst at the sane time. Then, the conduction electron is scavenged by the O_2 on the surface of the catalyst to form $O_2•^-$. The VB holes of AgBr/Bi_2WO_6 would attack MB to form intermediate products or pass to the VB of AgBr. The photocatalytic degradation reaction would subsequently take place, in which the intermediate products could transform and eventually decompose to CO_2 and H_2O by both the VB holes and $O_2•^-$ radicals. The reaction possibly includes the following:

$AgBr/Bi_2WO_6 + h\nu \rightarrow AgBr/Bi_2WO_6\ (e_{CB}^- + h_{VB}^+)$ ①

$AgBr/Bi_2WO_6(e_{CB}^-) + O_2 \rightarrow AgBr/Bi_2WO_6 + O_2•^-$ ②

$MB + h_{VB}^+\ [AgBr/Bi_2WO_6] \rightarrow$ intermediate products ③

$O_2•^- + MB \rightarrow$ intermediate products ④

Simultaneous photocatalytic reaction:

intermediate products+ $h_{VB}^+\ [AgBr/Bi_2WO_6]$ or $O_2•^- \rightarrow$

$CO_2 + H_2O + \ldots$ ⑤

4. Conclusion

Monodispersed AgBr QDs with the size of about 10 nm were deposited on the surface of 3D mesoporous Bi_2WO_6 nanoarchitectures by a simple precipitation-deposition process. The AgBr QDs decorated Bi_2WO_6 exhibits much enhanced photocatalytic activity in degradation of MB under visible light irradiation, which is more higher than that of pure Bi_2WO_6, and the content of AgBr QDs has an impact on the catalytic activity of AgBr-loaded Bi_2WO_6. The photocatalytic activity of as- prepared 2.0at%AgBr/Bi_2WO_6 exhibited the best photocatalytic activity. The mechanism of enhanced photocatalytic activity for was discussed. The enhanced activity of the as-fabricated AgBr/Bi_2WO_6 heterojunctions is attributed to the efficient separation of electron-hole pairs in AgBr/Bi_2WO_6 due to the formation of heterojunction between the two semiconductors. It was both O_2•- and photogenerated are the main reactive species responsible for the degradation of MB. Furthermore, AgBr/Bi_2WO_6 heterojunctions have highly stability and easy to be recycled, suggesting that the facile precipitation-deposition process to synthesize p-n heterojunctions could be a promising strategy to design new efficient photocatalysts for the water purification application and environmental remediation.

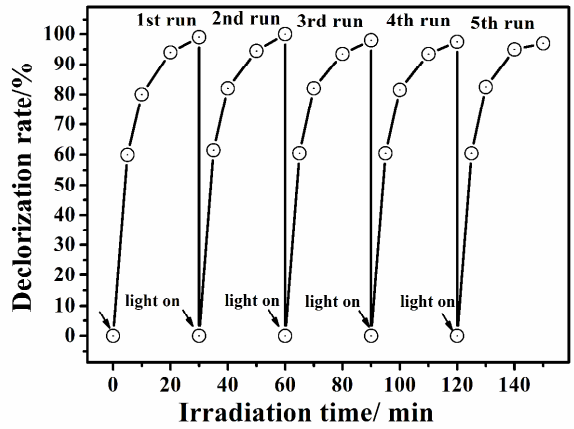

Fig. 10 The repeated experiments of photocatalytic degradation of MB on the AgBr/Bi_2WO_6 hierachical p-n nanojunction under visible light irradiation (initial concentration of MB, 10 mg·L^{-1}).

3.5 Stability of AgBr/Bi_2WO_6 heterojunctions. The stability of photocatalyst is important for its application. To demonstrate the potential applicability of AgBr/Bi_2WO_6 photocatalysts, the stability of as-prepared 2.0at%AgBr/Bi_2WO_6 heterojunctions nanoarchitecture was investigated. Fig.10 shows the results of a repeated experiment for the durability of MB degradation on 2.0at%AgBr/Bi_2WO_6. MB was quickly degraded after every cycle, suggesting that 2.0at%AgBr/Bi_2WO_6 showed relatively stable performance. After five recycles for photodegradation of MB, the catalyst did not exhibit any obvious loss of activity, as shown in Fig.10, indicating AgBr/Bi_2WO_6 heterojunctions nanoarchitecture has highly stability. Fig. S6 and Fig.S7 show the XRD and TEM image AgBr/Bi_2WO_6 photocatalyst patterns before and after used. It is found that there is no change in position and intensity of all diffraction peaks and there is no other phases detected in the XRD patterns of the photocatalyst. Moreover, the TEM image of used 2.0at%AgBr/Bi_2WO_6 photocatalyst has not found obvious change.

Acknowledgment

This work was supported by the National Natural Science Foundation of China (No.21373159). This work was also financially supported Science and Technology Department of Shaanxi Province(2013k11-08), Natural Science Foundation of Shaanxi Provincial Education Office (Grant No. 12JS117, 12JK0597, 2013JK0669) and the Key Industry Plan of Yan'an City (2011kg-13)

Supporting information available: A summary of literature reported photocatalyst for degradation of MB (Table S1), the schematic diagram of the photoreactor (Fig.S1), the nitrogen adsorption/adsorption isotherms and pore size distribution polt of as-prepared nest-like 3D Bi_2WO_6 architecture (Fig. S2), showing the comparison of the photocatalytic activity of

2.0at%AgBr/Bi_2WO_6 heterojunction structures, P25 and $TiO_{2-x}N_x$ (Fig. S3), the comparison of TEM image of 2.0at%AgBr/Bi_2WO_6 heterojunction with different AgBr content (Fig. S4), the effect of radical scavenger and a hole scavenger on the photocatlaytic activity of as-synthesized AgBr/Bi_2WO_6 photocatalyst (Fig. S5), and the comparison of XRD pattern and TEM image of 2.0at%AgBr nanodots loaded Bi_2WO_6 architecture before (Fig. S6) and after used (Fig. S7). This materials is available free of charge via the Internet.

References

1 M. R. Hoffmann, S. T. Martin, W. Choi and D. W. Bahnemann, *Chem. Rev.*, 1995, **95**, 69.
2 X. B. Chen and C. Burda. *J. Am. Chem. Soc.*, 2008, **130**, 5018.
3 X. G. Han, Q. Kuang, M. S. Jin, Z. X. Xie and L. S. Zheng, *J. Am. Chem. Soc.*, 2009, **131**, 3152.
4 X. Chen, S. Shen, L. Guo and S. S. Mao, *Chem. Rev.,* 2010, **110**, 6503.
5 X. Chen and S. S. Mao, *Chem. Rev.,* 2007, **107**, 2891.
6 S. Sakthivel and H. Kisch, *Angew. Chem. Int. Ed.*, 2003,**42**, 4908.
7 R. Fujishima, T. Morikawa, T. Okwaki, K. Aoki and Y. Taga, *Science,* 2001, **293**, 269.
8 W. Ho, C. J. Yu and S. Lee, *Chem. Commun.,* 2006, **10**, 1115.
9 J. Liu, Q, Yang, W. T. Yang, M. Z. Li and Y. L. Song, *J. Mater. Chem. A*, 2013, **1**, 7760.
10 M. A. Henderson, *Surf. Sci. Rep.*, 2011, **66**, 1185.
11 A. Kubacka, M. Fernandez-Garcia and G. Colon, *Chem. Rev.,* 2011, **112**, 1555.
12 S. Tamar, G. Pierre, C. Nicolas, C. Corinne, D. Olivier and B. Vlasta, C. J.Cristophe, J. Jean-Pierre, *J. Phys. Chem. C,* 2013, **117**, 22656.
13 M. D. Hernandez-Alonso, Fresno, S. Suarez and J. M. Coronado, *Energy. Environ. Sci.*, 2009, **2**,1231.
14 S. Y. Chai, Y. J. Kim, M. H. Jung, A. K. Chakra, D. W. Jung and W. I. Lee, *J. Catal.*, 2009, **262**, 144.
15 S. N. Chai, G. H. Zhao, Y. J. Wang, F. Q. Nong, M. F. Li and D. M. Li, *Environ. Sci. Technol.*, 2012, **46**, 10182.
16 S. N. Chai, G. H. Zhao, P. Q. Li, Y. N. Zhang, D. M. Li, *J. Phys. Chem. C* 2011, **115**, 18261.
17 A. Kudo and Y. Miseki, *Chem. Soc. Rev.*, 2009, **38**, 253.
18 Y. Q. Qu and X. F. Duan, *Chem. Soc. Rev.*, 2013,**42**, 2568.
19 L. Liang, Z. Jiang, H. H. Hai, R. J. Nicholls, T. C. Xiao, M. O. Jones and P.P. Edwards, *J. Catal.*, 2012, **293**, 116.
20 X. Zhang, L. Zhang, T. Xie and D. Wang, *J. Phys. Chem. C,* 2009, **113**, 7371.
21 H. G. Kim, P. H. Borse, J. S. Jang, E.D. Jeong, O. S. Jung, Y. J. Suh and J. S. Lee, *Chem. Commun.*, 2009, **39**, 5889.
22 S. Y. Chai, Y.J. Kim, M. H. Jung, A. K. Chakraborty, D. Jung and W. L. Lee, *J. Catal.*, 2009, **262**, 144.
23 Y. Lan, C. Hu, X. Hu and J. Qu, *Appl. Catal. B,* 2007, **73**, 354.
24 H. Cheng, B. Huang, P. Wang, Z. Wang, Z. Lou, J. Wang, X. Qin, X. Zhang and Y. Dai, *Chem. Commun.,* 2011, **47**, 7054.
25 C. Y. Wang, H. Zhang, F. Li and L. Y. Zhu, *Environ. Sci. Technol.*, 2010, **44**, 6843.
26 L.W. Zhang, Y. J. Wang, H. Y. Cheng, W. Q. Yao and Y. F. Zhu, *Adv. Mater.*, 2009, **21**, 1286.
27 H. B. Fu, C. S. Pan , W. Q. Yao and Y. F. Zhu, *J. Phys. Chem., B,* 2005, **109**, 22432.
28 L. S. Zhang, W. Z. Wang, Z. G. Chen, L. Zhou, H. L. Xu and W. Zhu, *J. Mater. Chem.*, 2007, **17**, 2526.
29 Y. H. Zhang, N. Zhang, Z.R. Tang and Y. J. Xu, *Chem. Sci.*, 2013, **4**, 1820.
30 D. V. Bavykin, V. N. Parmon, A. A. Lapkin and F. C. Walshi, *J. Mater. Chem.*, 2004, **14**, 3370.
31 J. G. Yu, H. G.Yu, B. Cheng and C. Traplis, *J. Mol. Catal. A,* 2006, **249**, 135.
32 Y.Y. Li, J. P.Liu, X. T. Huang and G. Y. Li, *Cryst. Growth. Des.*, 2007, **7**, 1350.
33 L. S. Zhang, W. Z. Wang, L. Zhou and H. L. Xu, *Small*, 2007, **3**, 1618.
34 L.W. Zhang and Y. F. Zhu, *Catal. Sci. Technol.*, 2012,**2**, 694.
35 H. F. Cheng, B. B. Huang, Y.Y. Liu, Z. Y. Wang, X. Y. Qin, X. Y. Zhang and Y. Dai, *Chem.Commun.*, 2012, **48**, 9729.
36 S. W. Liu and J. G. Yu, *J. Solid State Chem.*, 2008, **181**, 1048.
37 D. K. Ma, S. M. Huang, W. X. Chen, S. W. Hu, F. F. Shi and K. L. Fan, *J. Phys. Chem. C*, 2009,**113**, 4369.
38 X. N. Li, R. K. Huang, Y. H. Hu, Y.J. Chen, W.J. Liu, R.S. Yuan, and Z. H. Li. *Inorg. Chem.*, 2012, **51**, 6245.
39 Y. Huang and Z. H. Ai, *J. Phys. Chem. C,* 2010, **39**, 6342.
40 X. J. Dai, Y. S. Luo, W. D. Zhang and S. Y. Fu, *Dalton. Trans.*, 2010, **114**, 6342.
41 Y. Tian, G. M. Hua, N. Li, M. Fang and L. D. Zhang, *J. Alloys. Compds.*, 2011, **509**, 724.
42 R. Shi, G. L. Huang, J. Lin and Y. F. Zhu, *J. Phys. Chem. C* 2009, **113**, 19633.
43 C. Bhattacharya, H. C. Lee and A. J. Bard, *J. Phys. Chem. C*, 2013, **117**, 9633.
44 L. W. Zhang, Y. Man and Y. F. Zhu, *ACS Catal.*, 2011, **1**, 841.
45 M. Shang, W. Z. Wang, L. Zhang and H. L. Xu, *Mater. Chem. Phys.*, 2010, **120**, 155.
46 M. S. Gui, W. D. Zhang, Q. X. Su and C. H. Chen, *J. Solid. State Chem.*, 2011, **184**, 1977.
47 Q. C. Xu, D. V. Wellia, Y. H.Ng, R. Amal, and T. T. Y. Tan, *J. Phys. Chem. C*, 2011, **115**.7419.
48 M. Ge, Y. F. Li, Z. Zhou and W. Chen, *J. Phys. Chem. C,* 2011, **115**, 5220.
49 J. Tian, Y. H. Sang, G. W. Yu, H. D. Jiang, X. N. Mu and H. Liu, *Adv. Mater.*, 2013, **25**, 5074.
50 H. W. Huang, S. B. Wang, N. Tian and Y. H. Zhang, *RSC Adv.*, 2014, **4**, 5561.
51 Q. C. Xu, Y. H. Ng, Y. Zhang, J. S. C. Loo, R. Amal and T. T. Y. Tan, *Chem. Commun.*, 2011, **47**, 8641.
52 D. J. Wang, Zhen Y Z, Xue G L, F. Fu, X. M. Liu and D. S. Li, *J.Mater. Chem. C,* 2013, **1**, 4153.
53 D. J. Wang, G. L. Xue, Y. Z. Zhen, F. Feng and D. S. Li, *J. Mater. Chem.*, 2012, **22**, 4751.
54 L. S. Zhang, K. H. Wong, Z. G. Chen, J. C. Yu, J. C. Zhao, C. Hu, C. Y. Chan and P. K. Wong, *Appl. Catal. A: Gen.,* 2009, **363**, 221.
55 L. S. Zhang, K. H. Wong, H. Y. Yip, C. Hu, J. C. Yu, C. Y. Chan and P. K. Wong, *Environ. Sci. Technol.*, 2010, **44**, 1392.

56 S. Sakthivel, M. Janczarek and H. Kisch, *J. Phys. Chem. B* 2004, **108**, 19384.

57 J. H. Ryu, S. Y. Bang, W. S. Kim, G. S. Park, K. M. Kim, J. W. Yoon, K. B. Shim and N. Koshizaki, *J. Alloys. Compd.,* 2007, **411**, 146.

58 O. Lupan, Chow, L. K. Ono, B. R. Cuenya, G. Y. Chai, H. Khallaf, S. Park and A. Schulte, *J. Phys. Chem. C*, 2010, **114**, 12401.

59 L. Armelao, M. Fabrizio, S. Gialanella, and F. Zordan, *Thin Solid Films*, 2001, **394**, 89.

60 C. Hu, Y. Q.Lan, J. H.Qu, X. X.Hu and A. M.Wang, *J. Phys. Chem. B*, 2006, **110**, 4066.

61 H. Zhang, G. Wang, D. Chen, X. J. Lv and J. H. Li, *Chem. Mater*., 2008, **20**, 20555.

62 H. Xu, Y. G. Xu, H. M. Li, J. X. Xia, J. Xiong, S. Yin, C. J. Huang and H. L. Wan, *Dalton. Trans.,* 2012, **41**, 3387.

63 J. Li, H. Q. Fan and X. H. Jia, *J. Phys. Chem. C*, 2010, **114**, 14684.

64 J. Cao, B. Luo, H. Lin and S. Chen, *J. Hazard. Mater*., 2011, **190**, 700.

65 L. Zheng, Y. Zheng, C. Chen, Y. Zhen, X. Lin, Q. Zheng, K. Wei and J. Zhu, *Inorg. Chem*., 2009, **48**, 1819.

66 P. Wardman, *J. Phys. Chem. Ref. Data,* 1989, **18**, 1637.

67 J. Zhang, J. Sun, K. Maeda, K. Domen, P. Liu, M. Antonietti, X. Fu and X. Wang, *Energy Environ. Sci*., 2011, **4**, 675.

68 M. Long, W. Cai, J. Cai, B. Zhou, X. Cai and Y. Wu, *J. Phys. Chem. B,* 2006, **110**, 20211.

69 S. Shamaila, A. K. L. Sajjad, F. Chen and J. Zhang, *J. Colloid Interface Sci.,* 2011, **356**, 465.

70 M. A. Butler and D. S. Ginley, *J. Electrochem. Soc*., 1978,**125**, 228.

71 K. Fujihara, S. Izumi, T. Ohno and M. Matsumura, *J. Photochem*. *Photobiol*. *A*: *Chem*., 2009, **132**, 99.

72 V. Subramanian, E. E. Wolf and P. V. Kamat, *J. Am. Chem. Soc*., 2004, **126**, 4943.

73 Z. J. Zhang, W. Z. Wang, L. Wang and S. M. Sun, *ACS Appl. Interfaces* 2012, **4**, 593.

74 H. Q. Li, Y. M. Cui, X. C. Wu, H. Lin and W. S. Hong, *Acta Phys.-Chim. Sin*., 2012, **28**, 1985.

75 Q. Xiao, J. Zhang, C. Xiao and T. K. Tan, *Catal. Commun*., 2009, **9**, 1247.

76 S. J. Chen, J. H. Zhou, X. T. Chen, J. Li, L. H. Li, J. M. Hong, Z. L. Xue and X. Zeng, *Chem. Phys. Lett*., 2003, **375**, 185.

77 S. F. Wang, F. Gu, M. K. Lu, W. G. Zou, S. W. Liu, D. Xu, D. R. Yuan and G. J. Zhou, *J. Phys. Chem. Solid*, 2004, **65**, 1243.

78 P. F. Smet, J. Van Gheluwe, D. Poelman and R. L. Van Meirhaeghe, *J. Lumin*., 2003, **104**, 145.

79 S. Obregón Alfaro, A. Martínez-de la Cruz, *Appl. Catal. A: Gen*., 2010, **383**, 128.

80 A. Martínez-de la Cruz, S. Obregón Alfaro, *Appl. Catal. A: Gen*., 2010, **320**, 85.

81 M. Zhang, C.Chen, W. Ma and J. Zhao, *Angew. Chem. Int. Ed*., 2008, **37**, 9730.

82 Y.H. Zhang, N. Zhang, Z. R. Tang and Y. J. Xu, *Chem. Sci*., 2013, **3**, 2812.

83 Y.H. Zhang, N. Zhang, Z. R. Tang and Y. J. Xu, *Chem. Sci*., 2013, **4**, 1820.